Fission hindrance in hot ^{216}Th: Evaporation residue measurements

B. B. Back, D. J. Blumenthal, C. N. Davids, D. J. Henderson, R. Hermann, D. J. Hofman, C. L. Jiang,
H. T. Penttilä, and A. H. Wuosmaa

Argonne National Laboratory, Argonne, Illinois 60439
(Received 8 April 1999; published 25 August 1999)

The fusion evaporation-residue cross sections for ^{32}S+^{184}W have been measured at beam energies of $E_{beam}=$ 165, 174, 185, 196, 205, 215, 225, 236, 246, and 257 MeV using the ATLAS Fragment Mass Analyzer. The data are compared with statistical model calculations and it is found that a nuclear dissipation strength, which increases with the excitation energy, is required to reproduce the excitation function. A comparison with previously published data shows that the dissipation strength depends strongly on the shell structure of the nuclear system. [S0556-2813(99)02709-0]

PACS number(s): 25.60.Pj, 25.70.Jj

I. INTRODUCTION

Experimental studies of the time scale of fission of hot nuclei have recently been carried out using the emission rates of neutrons [1], γ rays [2], and charged particles [3] as ''clocks'' for the fission process. These experiments have shown that the fission process is strongly hindered relative to expectations based on the statistical model description of the process. The observed effects extend well beyond any uncertainties in the model parameters. It therefore appears that a dynamical description of the fission process at these energies is more appropriate [4] and that the experimental data are able to shed light on dissipation effects in the shape degree of freedom. However, these experiments are not very sensitive to whether the emission occurs mainly before or after the traversal of the saddle point as the system proceeds toward scission. Various dissipation models are, however, strongly dependent on the deformation and shape symmetry of the system. As an alternative to these methods we therefore measure the evaporation probability for hot nuclei formed in heavy-ion fusion reactions, which is sensitive only to the dissipation strength inside the fission barrier. As the hot system cools down by the emission of neutrons and charged particles there is a finite chance to undergo fission after each evaporation step. If the fission branch is suppressed due to dissipation there is therefore a strongly enhanced probability for survival which manifests itself as an evaporation residue cross section which is larger than expected from statistical model predictions. This effect depends, however, only on the dissipation strength inside the saddle point and may therefore provide the desired separation between presaddle and postsaddle dissipation.

In this paper, we report on recent measurements of evaporation residue cross sections for the ^{32}S+^{184}W system over a wide range of beam energies using the Argonne Fragment Mass Analyzer (FMA). In Sec. II we describe the experimental procedure followed by a discussion of the measurements of absolute evaporation residue cross section in Sec. III. The results are compared to statistical model calculations and other relevant data in Sec. IV followed by the conclusion, Sec. V.

II. EXPERIMENTAL ARRANGEMENT

The measurements were carried out using ^{32}S-beams from the ATLAS superconducting linac at Argonne National Laboratory. The cross sections for evaporation residues produced in the ^{32}S+^{184}W reaction were measured at beam energies of 165, 174, 185, 195, 205, 215, 225, 236, 246, and 257 MeV. Targets of isopically separated ^{184}W with thickness 200 μg/cm^2 on a 100 μg/cm^2 carbon backing were used. The Argonne Fragment Mass Analyzer [5] was used for identification of evaporation residues. A schematic illustration of the setup is shown in Fig. 1.

In these experiments a sliding seal target chamber was used, which allows for measurements at angles away from 0°. This is required in order to obtain the angular distributions for integration of the total evaporation residue cross section. Elastically scattered S ions were registered in a Si detector placed at 30° relative to the beam axis with a solid angle of $\Omega_{mon}=0.249$ msr. These data were used for normalization purposes. A 40 μg/cm^2 carbon foil was placed 10 cm downstream from the target to reset the charge state of
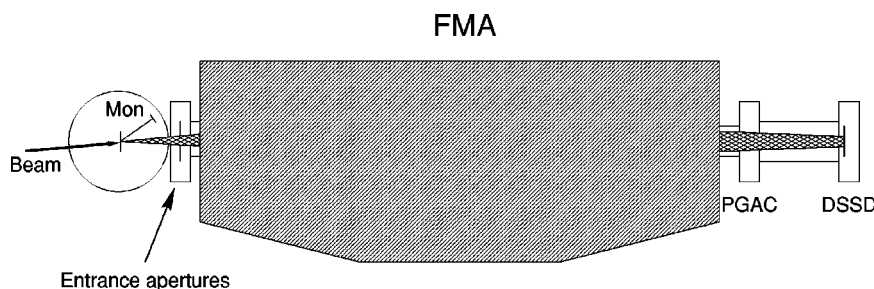

FIG. 1. Schematic illustration of the Argonne Fragment Mass Analyzer. The beam enters from the left.
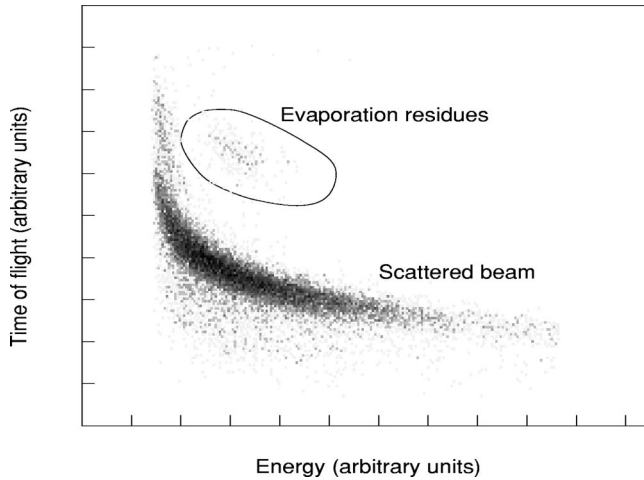
FIG. 2. Separation of evaporation residues from scattered beam particles on the basis of time-of-flight and energy.
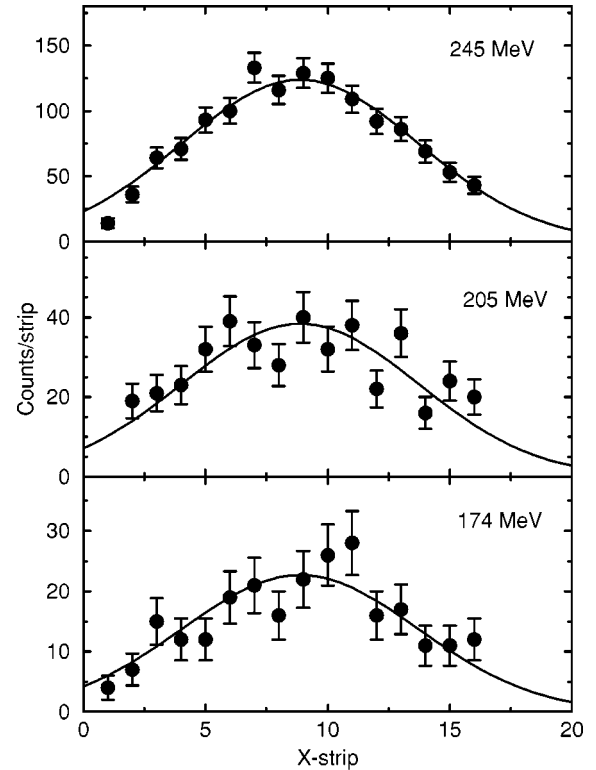

FIG. 3. The horizontal position distribution on the Si-strip detector is shown for three beam energies. The solid curves represent Gaussian fits to the data, from which the detection efficiency is estimated.

reaction products, which may be abnormally highly charged as a result of Auger electron emission following the γ decay of short-lived isomers.

A square entrance aperture for the FMA covering $\theta, \phi = 4.5° \times 4.5° (\Omega_{FMA} = 6.24$ msr) was used. Reaction products transmitted through the FMA were dispersed in M/q (mass/charge) at the focal plane, where the spatial distribution was measured by a thin x-y position sensitive avalanche detector. When the FMA was placed at $0°$ some settings of the electrostatic and magnetic fields of the instrument allows beam particles scattered off the anode of the first electrostatic dipole, ED1, to be transported to the focal plane (presumably after a subsequent forward scattering in the vacuum chamber of the magnetic dipole MD1). When measuring small cross sections, as in the present study, it is therefore mandatory to achieve a clean separation between evaporation residues and beam particles. This was achieved by measuring their flight-time over the 40 cm distance to a double-sided Si strip detector (DSSD) placed behind the focal plane. This detector has a total active area of 5×5 cm^2 and is divided into 16 strips on both the front and rear surface arranged orthogonally to each other. The information on the particle mass obtained from the time-of-flight and energy measurement provided by the Si-detector gave a clean discrimination against the scattered beam as illustrated in Fig. 2. The efficiency for transporting evaporation residues from the focal plane to the Si-detector was determined from the spatial distribution over the face of the DSSD detector as shown in Fig. 3 for these beam energies. By Gaussian extrapolation of the distribution beyond the edge of the detector it is estimated that this efficiency is around $\epsilon_{PPAC-Si} = 87\%$.

The transport efficiency of the FMA as a function of the mass, energy, amd charge-state of the ion has been determined in a separate experiment [6,7].

III. CROSS SECTIONS

The evaporation residue cross section for the ^{32}S + ^{184}W reaction was measured for beam energies in the range $E_{beam} = 165–257$ MeV. Evaporation residues were identified

by time-of-flight and energy measurement using the focal plane PPAC detector and the Si-strip detector placed ca. 40 cm behind the focal plane. The charge state distributions, which were measured at three beam energies, are shown in Fig. 4. The dashed curves represent the formula of Shima *et al.* [8], whereas a somewhat better fit to the data is given by the Gaussian fit (solid curves) with a fixed standard deviation of $\sigma = 3$. The arrows indicate the charge state setting of the FMA used for the cross section measurement. The derivation of the evaporation residue cross section at intermediate beam energies is based on an interpolation between these measured charge state distributions.

Since the FMA disperses in M/q at the focal plane there will be cases of ambiguities in the mass identification, since overlaps between lighter mass products from one charge state, q, will invariably overlap with heavier products from the neighboring charge state, $q + 1$, when compound nuclei with high excitation energy are studied; see Fig. 5. We are not able to resolve this ambiguity with the present setup, and have therefore obtained the cross sections by integrating all counts that fall between the positions for $M/(q - \frac{1}{2})$ and $M/(q + \frac{1}{2})$ along the focal plane. Since the FMA is set up for the most abundant charge state, q and mass, M, we expect that the loss of residues with charge state, q, and masses that fall outside this window is compensated by the acceptance of residues with charge states, $q + 1$ and $q - 1$ that fall inside this window.
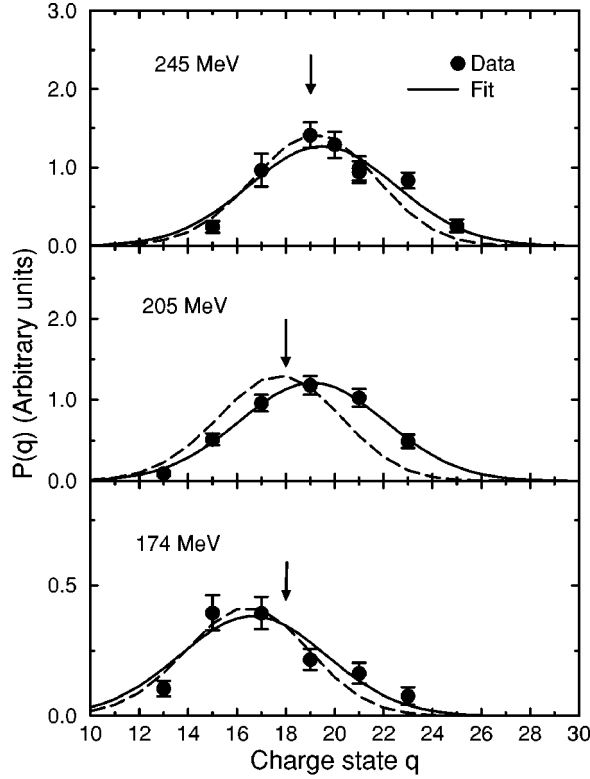
FIG. 4. Charge-state distribution, $P(q)$, of evaporation residues from the ^{32}S + ^{184}W reaction measured at three beam energies.

A. Detection efficiency

The transport efficiency as a function of recoil energy and mass relative to the setting for the FMA has been measured for monoenergetic particles by observing the recoils from elastic scattering of ^{32}S + ^{197}Au, ^{208}Pb, ^{232}Th [6]. To correctly estimate the transport efficiency for evaporation residues, which have an extended energy distribution, it is necessary to fold the energy distribution with the measured acceptance curve. The energy distribution was not measured directly in the present experiment, but the yield of residues as a function of the energy setting of the FMA was measured as shown in Fig. 6 (top panel). In principle, since the energy acceptance of the FMA is known, it should be possible to convert this measurement into an energy distribution with some accuracy.

We have, however, used a slightly different method which incorporated both this measurement and the measurement of the angular distributions. Assuming that both the angular distribution of evaporation residues and their energy distribution at 0° arise from isotropic multiparticle emission from the hot compound nucleus, these two entities are related by the kinematics of the particle decay cascade. We assume that the recoil energy distribution is isotropic in the center-of-mass system and that it has a Maxwellian form, namely,

$$\frac{dP}{dE_{\text{c.m.}}} = \frac{2}{\sqrt{\pi}} \frac{\sqrt{E_{\text{c.m.}}}}{a^{3/2}} \exp(-E_{\text{c.m.}}/a), \qquad (1)$$

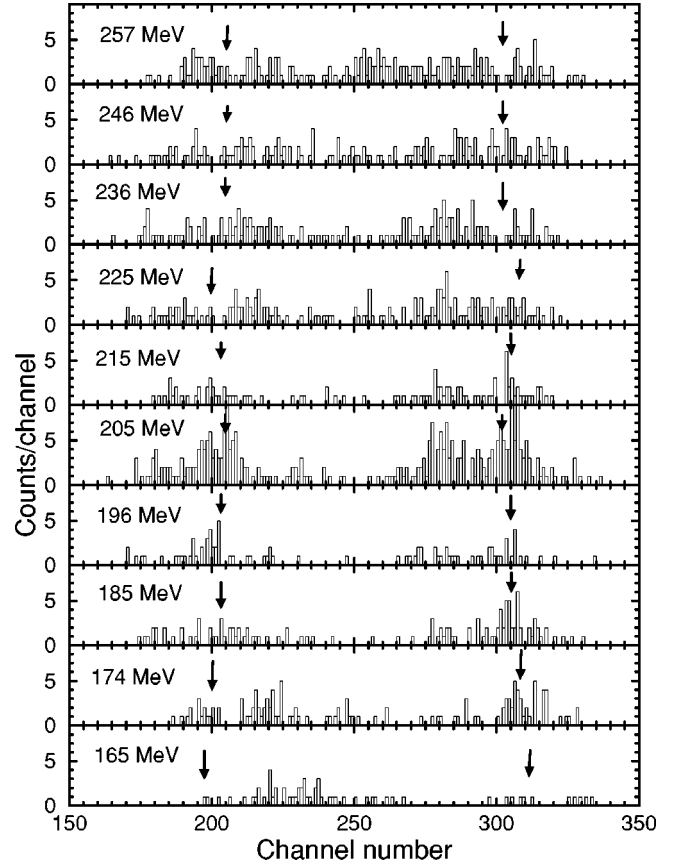where $E_{\text{c.m.}}$ is the recoil energy in the center-of-mass system

FIG. 5. Horizontal position distribution of evaporation residues along the focal plane, which scales with M/q. The arrows indicate the region of integration from $M/(q+\frac{1}{2})$ to $M/(q-\frac{1}{2})$.

and $a = \frac{2}{3}\langle E_{\text{c.m.}}\rangle$ is two thirds of its average value. The energy distribution in the laboratory system at $\theta = 0°$ is then

$$\left.\frac{dP}{dE_{\text{lab}}}\right|_{0°} = \frac{1}{2}\left(\frac{1}{\pi a}\right)^{3/2} \sqrt{E_{\text{lab}}} \exp[-(\sqrt{E_{\text{lab}}} - \sqrt{E_{\text{CN}}})^2/a].$$
$$(2)$$

Here, E_{CN} is the laboratory energy of the compound nucleus prior to the particle evaporation cascade. A small correction to E_{CN} arising from the mass loss due to particle evaporation has been ignored in Eqs. (1)–(3). Similarly we find the angular distribution

$$\frac{dP}{d\Omega_{\text{lab}}} = \frac{1}{2}\left(\frac{1}{\pi a}\right)^{3/2} \int_0^\infty \sqrt{E_{\text{lab}}} \exp[-(E_{\text{lab}} + E_{\text{CN}}$$
$$-2\sqrt{E_{\text{lab}}E_{\text{CN}}} \cos\theta)/a] dE_{\text{lab}}. \qquad (3)$$

We find that a value of $a = 0.5$ MeV gives a good representation of both the transmission as a function of the energy setting of the FMA, E_{FMA} and the measured angular distribution; see Fig. 6. For the angular distribution we have also taken the effects of multiple scattering in the target and backing material as well as the charge state reset foil into account. This increases the width of the angular distribution somewhat and results in good agreement with the data as shown
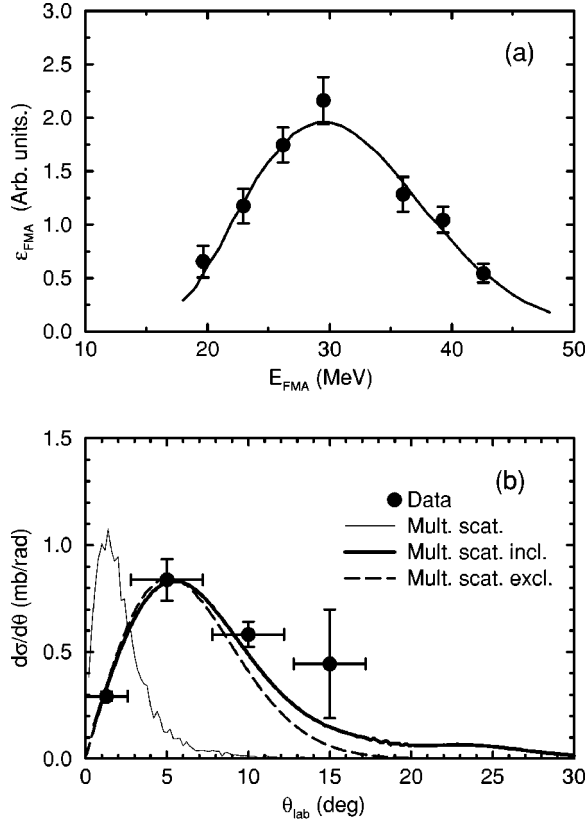
FIG. 6. Top panel (a): Transport efficiency ϵ_{FMA} (arbitrary units) for evaporation residues from 245 MeV ^{32}S$+^{184}$W measured with the FMA optimized for $M=208$ and $q=19$ and different energy E_{FMA} settings (solid points). The solid curve results from a calculation detailed in the text. Bottom panel (b): Angular distribution $d\sigma/d\theta_{lab}$ for the same reaction is shown as solid points (assuming a transport efficiency of $\epsilon=1.0$ to the focal plane). The thick solid and dashed curves represent calculations to fit simultaneously the transport efficiency data [panel (a)] and the angular distributions with and without multiple scattering in target and reset foils, respectively. The thin curve shows the calculated multiple scattering distribution.

by the solid curve in Fig. 6(b). This value of $a=0.5$ MeV corresponds to a transport efficiency of the FMA for evaporation residues of $\overline{\epsilon_{FMA}}\approx0.60$; see Table I.

B. Angular distributions

The angular distributions of evaporation residues were measured at three beam energies utilizing the sliding-seal target chamber for the FMA. Differential cross sections, $d\sigma/d\Omega$, as a function of the mean angle, $\langle\theta_{lab}\rangle$, relative to the beam axis are shown in the left side panel of Fig. 7. The right side panel shows the cross sections converted to $d\sigma/d\theta$, which is relevant for the angular integration of the total evaporation residue cross section. The angle integrated cross sections are thus derived from a fit to the data expressed in terms of $d\sigma/d\theta$ using the function $2\pi\sin\theta d\sigma/d\Omega_{lab}$. The curves shown in the left side panel of Fig. 7 are computed by removing the $2\pi\sin\theta$ term. We observe that these latter curves underrepresent the differen-

TABLE I. Reaction parameters and total evaporation residue cross section. E'_{CN} is the kinetic energy of the fused ^{216}Th system corrected for energy losses in the target material, backing, and the charge state reset foil, A_{ER} is the average mass of the evaporation residue, E_{FMA} is the energy setting of the FMA, $\overline{\epsilon_{FMA}}$ is the resulting average transport efficiency through the FMA for the assumed distribution of evaporation residues, and σ_{ER} is the total evaporation residue cross section.

E_{beam} (MeV)	E'_{CN} (MeV)	A_{ER} (u)	a (MeV)	E_{FMA} (MeV)	$\overline{\epsilon_{FMA}}$	σ_{ER} (μb)
165	19.3	212	0.34	22	0.61	72 ± 14
174	20.4	212	0.36	23	0.60	47 ± 10
185	21.7	211	0.38	25	0.61	63 ± 13
196	23.0	210	0.41	26	0.60	68 ± 14
205	24.1	209	0.43	27	0.60	75 ± 15
215	25.3	208	0.44	29	0.61	103 ± 20
225	26.5	207	0.46	30	0.61	115 ± 23
236	27.9	206	0.48	31	0.60	125 ± 25
246	29.1	205	0.50	33	0.61	190 ± 38
257	30.4	204	0.52	35	0.60	175 ± 35

tial cross section at small angles indicating that the angular distribution really has two components. However, we do not feel that the data are of sufficient quality to allow for a reliable separation of two components and by observing the fits to the $d\sigma/d\theta$ data it is clear that only a very small error could arise from this simplification.

The data shown in Fig. 7 are corrected for the efficiency for transporting evaporation residues through the FMA. We estimate this transport efficiency, ϵ_{FMA}, by folding the energy distribution of the evaporation residues with the energy acceptance of the FMA, which was measured by Back *et al.*
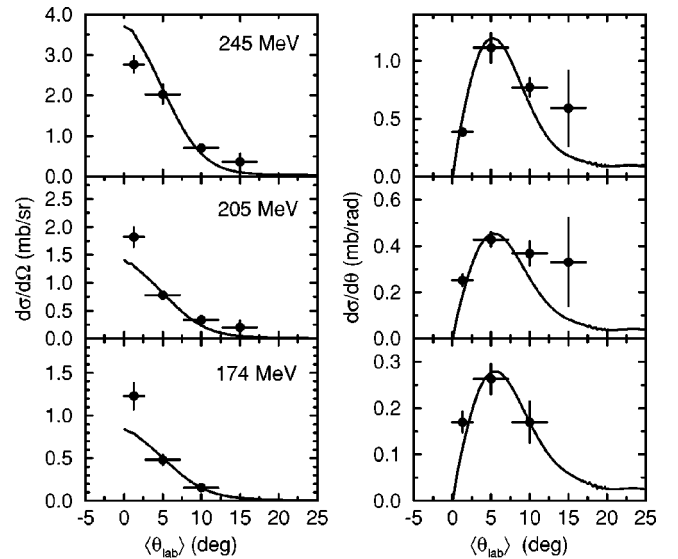

FIG. 7. Right panels: Experimental angular distributions $d\sigma/d\theta_{lab}$ are compared with calculations (solid curves), see text, at three beam energies. Left panels: the same data and curves are shown in a $d\sigma/d\Omega$ representation.

[6] for the entrance aperture used in this experiment. The mean energy of the compound system, $E'_{\rm CN}$ (corrected for the energy losses in the target material, backing and the reset foil), is determined from the reaction kinematics and listed in Table I. The parameter, $a = \frac{2}{3}\langle E_{\rm c.m.}\rangle$ was determined to have a value of about $a \approx 0.5$ for the $E_{\rm beam} = 246$ MeV point by simultaneously fitting the angular distribution of evaporation residues and a scan of the energy setting of the FMA; see Fig. 6. The value of a was for the other beam energies scaled according to $a \propto \sqrt{E^*}/22.4$, which was found to reproduce also the angular distributions measured at $E_{\rm beam} = 174$ and 205 MeV; see Fig. 7. Here E^* is the excitation energy of the compound system.

C. Total evaporation residue cross sections

The total evaporation residue cross section, $\sigma_{\rm ER}$, is obtained from the measurement of the differential cross section at $\theta = 5°$, which was performed at all beam energies. The ratio, $f(E_{\rm beam}) = \sigma_{\rm ER}/(d\sigma_{\rm ER}/d\theta)$, of the angle integrated cross section, $\sigma_{\rm ER}$, to the measured differential cross section, $(d\sigma_{\rm ER}/d\theta)$, at $\theta = 5°$, is obtained by smooth interpolation between the values of $f(E_{\rm beam}) = 0.089$, 0.088, and 0.086 rad obtained from the angular distribution measurements at $E_{\rm beam} = 174$, 205, and 246 MeV, respectively. The total evaporation residue cross sections are then given by

$$\sigma_{\rm ER} = f(E_{\rm beam})\frac{d\sigma(5°)}{d\theta}$$

$$= f(E_{\rm beam})\frac{N_{\rm ER}(5°)}{N_{\rm mon}}\frac{\Omega_{\rm mon}}{\Omega_{\rm FMA}}2\pi\sin(5°)$$

$$\times \frac{d\sigma_{\rm Ruth}}{d\Omega}(30°)\frac{1}{\epsilon_{\rm FMA}\epsilon_{\rm PPAC\text{-}Si}P(q)}, \qquad (4)$$

where, $N_{\rm ER}(5°), N_{\rm mon}$ are the number of evaporation residue counts observed at the FMA focal plane Si detector, and the number of elastically scattered ^{32}S ions registered in the monitor detector, respectively. The differential Rutherford cross section in the laboratory system is denoted $d\sigma_{\rm Ruth}/d\Omega$, and $P(q)$ is the fraction of evaporation residues in the charge state, q, for which the FMA was tuned. The charge state fraction, $P(q)$, was obtained by interpolation of the central charge state, q_0 resulting from the fits to the measured distributions with a Gaussian with a standard deviation of $\sigma = 3$ charge state units.

The resulting evaporation residue cross sections for the ^{32}S + ^{184}W reaction are shown as filled circles in Fig. 8 and listed in Table I. The measurements are assigned a systematic error of 20%, mainly due to the procedure for estimating the transport efficiency through the FMA.

Fissionlike cross sections and a derived estimate of the complete fusion cross sections for the ^{32}S + ^{182}W reaction are shown as open circles [9,10] and open squares [10], respectively, along with theoretical calculations using a modified Extra Push model [11].
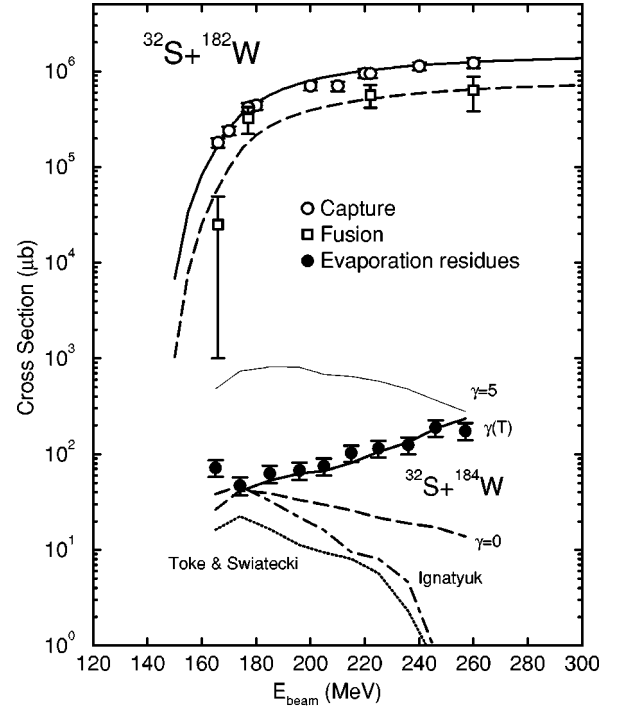

FIG. 8. Evaporation residue cross sections for the reaction ^{32}S + ^{184}W (solid points) are compared with statistical model calculations with and without fission hindrance (see text). The capture cross section (fission + quasifission) (open circles) and estimates of the complete fusion (open squares) cross sections are shown in comparison with theoretical calculations (short dashed and long-dashed curves); see text. The latter calculations were used to provide the initial spin distribution for the statistical model calculation of the evaporation residue cross section.

IV. COMPARISON WITH STATISTICAL MODEL CALCULATIONS

In Fig. 8, the evaporation residue data are compared with a statistical model calculation obtained with the code CASCADE (long dashed curve labeled $\gamma = 0$) using Sierk fission barriers [12] scaled by a factor of 0.9 to approximately account for the cross section at low beam energies, and using level density parameters of $a_n = a_f = A/8.8$ MeV^{-1}. We observe that the measured cross section increases with beam energy, whereas the statistical model predicts a decreasing cross section because of an increased probability for fission during the longer evaporation cascades. For comparison we have also performed CASCADE calculations using level density parameters of $a_n = A/8.68$ MeV^{-1} and $a_f = A/8.49$ MeV^{-1} as suggested by Tōke and Swiatecki [13] (dotted curve), and $a_n = A/11.26$ MeV^{-1} and $a_f = A/11.15$ MeV^{-1} by Ignatyuk *et al.* [14] (dotted-dashed curve). Using these values results in an even sharper decrease of the predicted evaporation residue cross section with beam energy as shown in Fig. 8. This is a consequence of the fact that the fission decay rate increases more rapidly with excitation energy when values of $a_f > a_n$ are used. Although it is expected that $a_f > a_n$ on rather firm theoretical grounds we have, however, used the standard values of $a_f = a_n$

=$a/8.8$ in order to be able to compare to other works, where this value was used in the analysis.

We hypothesize that the observed increase of the measured evaporation residue cross section with excitation energy, which is at variance with the statistical model calculations, can be attributed to an increased hindrance of the fission motion with excitation energy. Fission hindrance at high excitation has previously been shown to explain observations of enhanced emission of prescission neutrons [1], charged particles [3], and γ rays [2], as well as recent observation of an enhanced survival probability of excited target recoils from deep inelastic scattering reactions [15].

The inclusion of friction in the fission motion results in a modification of the normal Bohr-Wheeler expression [16] for the fission decay width, Γ_f^{BW} as pointed out by Kramers [17], i.e.,

$$\Gamma_f^{Kramers} = \Gamma_f^{BW}(\sqrt{1+\gamma^2} - \gamma)[1 - \exp(-t/\tau_f)], \quad (5)$$

where $\gamma = \beta/2\omega_0$ is a reduced nuclear friction coefficient, and τ_f is a charactistic time for the building of the fission flux over the saddle point. β denotes the reduced dissipation constant and ω_0 describes the potential curvature at the fission saddle point. The modification to the Bohr-Wheeler expression for the fission width thus consists of an overall reduction given by the so-called Kramers factor, $\sqrt{1+\gamma^2} - \gamma$, as well as a time dependent in-growth of the fission rate given by the factor $1 - \exp(-t/\tau_f)$ [18]. These modifications to the fission decay width has been incorporated into the CASCADE statistical model code in an approximate way [19], which has, however, been shown [20] to be very accurate over the applied range of parameters.

Because the evaporation residue cross section is such a small fraction of the complete fusion cross section we find that it is very sensitive to the nuclear viscosity of the system inside the barrier. The thin solid curve in Fig. 8 represent a statistical model calculation where the effects of viscosity are included using a linear normalized dissipation coefficient of $\gamma = 5$, corresponding to a strongly overdamped motion in the fission degree of freedom. This is approximately the dissipation strength expected from the one-body dissipation mechanism [21]. We see that this leads to an increase of about a factor of 10–20 in the evaporation residue cross section relative to the pure statistical model estimate (long dashed curve), but the overall shape of the excitation function is virtually unchanged. Within this framework it therefore appears that the viscosity (or dissipation) increases rather rapidly over this range of beam energies, i.e., from 200 to 260 MeV, which corresponds to an excitation energy range of $E_{exc} = 85-136$ MeV. Similar effects have been observed in studies of prescission γ rays [2] albeit in that case it appears to take place over an even smaller excitation energy interval.

In order to deduce the temperature dependence of the dissipation strength in the fission degree of freedom $\gamma(T)$ that reproduces the observed increase of the evaporation residue cross section, we have performed a series of calculations at each beam energy, varying the value of γ to reproduce the measured cross section. This procedure leads to the thick solid cross section curve going through the data points in
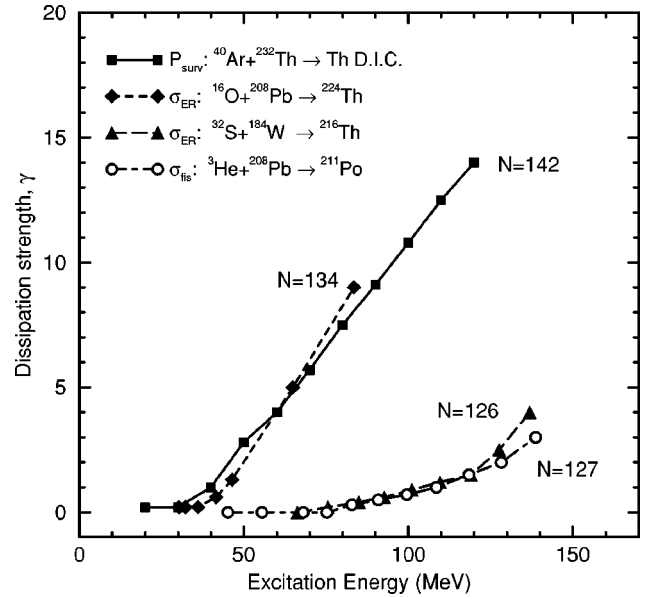

FIG. 9. Comparison of the fission dissipation strength, γ, required to reproduce different data.

Fig. 8; the corresponding values of $\gamma(T)$ are plotted as solid triangles in Fig. 9. Note that there is some inconsistency in this approach because the value of the dissipation strength is *not* allowed to vary as the system cools down during the particle evaporation cascade. Rather, the dissipation strength is kept constant throughout the cascade with the value needed to fit the measured evaporation residue cross section for this particular beam energy. Although this has been recognized as a shortcoming of these calculations, we have employed this procedure to be able to compare to other published data analyzed in the same way.

V. DISCUSSION

The dissipation strength in the fission process has recently been measured by several methods, and it is of interest to compare these different results. In Fig. 9 we show the normalized dissipation strength parameter, γ, obtained from the analysis of (1) the survival probability of Th-like nuclei excited in deep-inelastic scattering reaction of 400 MeV ^{40}Ar $+ ^{232}$Th [15] (solid squares), (2) the evaporation residue cross section and prescission γ-ray emission from the ^{16}O $+ ^{208}$Pb [22,23] (solid diamonds), (3) the present data (solid triangles), and (4) the fission cross section for ^{3}He$+ ^{208}$Pb reaction [24,25] (open circles). We observe that the dissipation strength required to reproduce the different data falls into two groups, namely one which increases rather sharply above an excitation energy of $E_{exc} \sim 40$ MeV, and another group that increases slowly only above $E_{exc} \gtrsim 80$ MeV.

It is interesting to note that this behavior may be related to the shell structure of the compound system. The two systems that have a closed (or nearly closed) neutron shell at $N = 126$ show only moderate fission dissipation strength up to high excitation energy, whereas the midshell systems with $N = 134$, 142 display a strong increase in γ above $E_{exc} \sim 40$ MeV.

Recently, there has been much theoretical interest in the study of the dynamics of the fission process, both in terms of the description of experimental observables on the basis of phenomelogical assumptions of the dissipation strength [26,27] as well as more fundamental theories for the dissipation mechanism itself [28–31]. Although the overall dissipation strength found to reproduce the present data is in fair agreement with estimates based on the simple one-body dissipation model, namely $\gamma \approx 5$–6 the rather striking increase with excitation energy (or temperature) is unexplained within this mechanism, which has no temperature dependence. It is interesting to note that the linear response theory approach [28] appears to predict the increase in dissipation strength although the present development level of this theory is not directly applicable for comparison with the experimental data.

VI. CONCLUSION

Measurements of evaporation residue cross sections for heavy fissile systems are shown to provide rather direct evidence for the fission hindrance (or retardation) which is caused by strong nuclear dissipation in the fission degree of freedom for hot nuclei. The data obtained for the ^{32}S $+^{184}$W system show an increasing evaporation cross section with excitation energy, whereas a decrease is expected on the basis of statistical model considerations and calculations. The data indicate an increase in the linear normalized dissipation coefficient γ from $\gamma = 0$ at $E_{\text{exc}} = 85$ MeV to $\gamma = 5$ at $E_{\text{exc}} = 135$ MeV. Although hints of such an increase have been obtained within the framework of linear response theory, no direct comparison can be made with the experimental data. Further study, both experimental and theoretical, of this phenomenon is warranted.

[1] D. Hinde *et al.*, Phys. Rev. C **45**, 1229 (1992).

[2] D. Hofman *et al.*, Phys. Rev. Lett. **72**, 470 (1994).

[3] J. Lestone *et al.*, Phys. Rev. Lett. **70**, 2245 (1993).

[4] P. Fröbrich *et al.*, Nucl. Phys. **A556**, 281 (1993).

[5] C.N. Davids *et al.*, Nucl. Instrum. Methods Phys. Res. B **70**, 358 (1992).

[6] B.B. Back *et al.*, Nucl. Instrum. Methods Phys. Res. A **379**, 206 (1996).

[7] H. Wollnik *et al.*, Nucl. Instrum. Methods Phys. Res. A **258**, 408 (1987).

[8] K. Shima *et al.*, Nucl. Instrum. Methods Phys. Res. **200**, 605 (1982).

[9] B.G. Glagola *et al.*, Phys. Rev. C **29**, 486 (1984).

[10] J.G. Keller *et al.*, Phys. Rev. C **36**, 1364 (1987).

[11] J. Tōke *et al.*, Nucl. Phys. **A440**, 327 (1985).

[12] A. Sierk, Phys. Rev. C **33**, 2039 (1986).

[13] J. Tōke and W.J. Swiatecki, Nucl. Phys. **A372**, 141 (1981).

[14] A.V. Ignatyuk *et al.*, Nucl. Phys. **A593**, 519 (1995); Yad. Fiz. **21**, 1185 (1975) [Sov. J. Nucl. Phys. **21**, 612 (1975)].

[15] D.J. Hofman *et al.* (unpublished).

[16] N. Bohr and J.A. Wheeler, Phys. Rev. **56**, 426 (1939).

[17] H.A. Kramers, Physica (Amsterdam) **7**, 284 (1940).

[18] P. Grangé, Li Jun-Qing, and H.A. Weidenmüller, Phys. Rev. C **27**, 2063 (1983).

[19] R. Butsch, D.J. Hofman, C.P. Montoya, P. Paul, and M. Thoennessen, Phys. Rev. C **44**, 1515 (1991).

[20] B. Back, in *Proceedings of the International School-Seminar on Heavy Ion Physics*, Dubna, Russia, 1993, edited by Y. Oganessyan (Dubna Press, Russia, 1993).

[21] J. Blocki, Y. Boneh, J.R. Nix, J. Randrup, M. Pobel, A.J. Sierk, and W.J. Swiatecki, Ann. Phys. (N.Y.) **113**, 330 (1978).

[22] K.-T. Brinkmann *et al.*, Phys. Rev. C **50**, 309 (1994).

[23] D.J. Hofman, B.B. Back, and P. Paul, Nucl. Phys. **A599**, 23c (1996).

[24] Th. Rubehn *et al.*, Phys. Rev. C **54**, 3062 (1996).

[25] B. B. Back *et al.*, *Proceedings of the ''International Conference on Fission and Properties of Neutron-rich Nuclei,''* Sanibel Island, 1997 (World Scientific, Singapore, 1998).

[26] P. Fröbrich and I.I. Gontchar, Phys. Rep. **292**, 131 (1998).

[27] A.K. Dhara, K. Krishan, C. Bhattacharya, and S. Bhattacharya, Phys. Rev. C **57**, 2453 (1998).

[28] H. Hofman, F.A. Ivanyuk, and S. Yamaji, Nucl. Phys. **A598**, 187 (1996).

[29] V.M. Kolomietz, V.A. Plujko, and S. Shlomo, Phys. Rev. C **54**, 3014 (1996).

[30] P. Magierski, J. Skalski, and J. Blocki, Phys. Rev. C **56**, 1011 (1997).

[31] T. Mukhopadhyay and S. Pal, Phys. Rev. C **56**, 296 (1997).